4-15-2020

Structure-Strength Relations of distinct MoN Phases from First-Principles Calculations

Cheng Lu
China University of Geosciences, lucheng@calypso.cn

Changfeng Chen
University of Nevada, Las Vegas, changfeng.chen@unlv.edu

Repository Citation

Lu, C., Chen, C. (2020). Structure-Strength Relations of distinct MoN Phases from First-Principles Calculations. *Physical Review Materials, 4*(4), 1-7. American Physical Society.
http://dx.doi.org/10.1103/PhysRevMaterials.4.044002

Structure-strength relations of distinct MoN phases from first-principles calculations

Cheng Lu [1,2,*] and Changfeng Chen [2,†]

[1] *School of Mathematics and Physics, China University of Geosciences (Wuhan), Wuhan 430074, China*

[2] *Department of Physics and Astronomy, University of Nevada, Las Vegas, Nevada 89154, USA*

(Received 2 February 2020; accepted 23 March 2020; published 15 April 2020)

Molybdenum mononitrides (MoN) exhibit superior strength and hardness among the large class of transition-metal light-element compounds, but the underlying atomistic mechanisms for their outstanding mechanical properties and the variations of those properties among various MoN phases adopting different crystal structures remain largely unexplored and require further investigation. Here we report first-principles calculations that examine the stress-strain relations of these materials, and systematically compare results under pure and indentation shear deformations. In particular, we examine the distinct bonding structures and the associated mechanical properties in four different crystal phases of MoN that have been experimentally synthesized and stabilized under various physical conditions. Our results reveal evolution patterns of bonding configurations and the resulting structural deformation modes in these MoN phases, which produce diverse stress responses and unexpected strength variations. These findings elucidate the structural and bonding characters that are responsible for the rich and distinct mechanical properties in various MoN structures, providing insights for understanding the experimentally observed phenomena and further exploring advanced superhard materials among the promising transition-metal nitrides, borides, and carbides.

DOI: 10.1103/PhysRevMaterials.4.044002

I. INTRODUCTION

Transition metal (TM) nitrides constitute a remarkable class of materials, which have drawn considerable interest and attention because of their excellent physical properties, such as low electrical resistivity, high melting point, superconductivity, and high strength and hardness [1–10]. This class of materials has a wide range of scientific and industrial applications ranging from wear-resistant coatings to cutting tools. The synthesis of bulk and high-quality TM nitrides, however, presents a technical challenge since direct reactions of transition metals with nitrogen gas is unfavorable. In general, it is more difficult to break the strong N#N triple bond and form a stable compound with TM elements compared to that of the corresponding oxides, borides, and carbides. Among various TM nitrides, MoN is one of the most promising hard materials with excellent mechanical and electronic properties [6,10]. Intense experimental and theoretical studies have been performed in the past few years [10–15]. MoN has been reported to crystallize in a variety of phases depending on the synthesis conditions and methods. It is commonly accepted that TM mononitrides often crystallize in a cubic rock-salt structure (B1-type). However, the B1-type MoN is thermodynamically unstable and does not exist in the equilibrium phase diagram of the Mo-N binary systems at ambient condition [14]. There are currently at least four known crystal structures of MoN: three different forms of the hexagonal structures (δ_1-MoN, δ_2-MoN, and δ_3-MoN) [15] and one cubic structure (γ-MoN) [16], as shown in Fig. 1.

The δ_1-MoN belongs to the space group $P\bar{6}m2$ configuration [15] with lattice parameters of $a = 2.8512$ Å and $c = 2.7823$ Å. It has been assigned to a tungsten-carbide-like structure, which Mo atoms occupy the 1*a* Wyckoff sites (0.000, 0.000, 0.000) and N atoms on 6*c* (0.6667, 0.3333, 0.5000). The δ_2-MoN crystallizes in a NiAs-type structure with lattice constants of $a = 5.729$ Å, $c = 5.604$ Å, and a space group of $P6_3/mmc$ symmetry [15]. It shows a six-fold N coordination for each Mo atom. The hexagonal layers of Mo atoms are stacked along the *c* axis, and N atoms are orderly arrayed in the *ab* plane and also stacked along the *c* axis. This structure contains two Mo atoms occupying the sites at 2*a* (0.000, 0.000, 0.000) and two N atoms at 2*c* (0.3333, 0.6667, 0.2500). The δ_3-MoN adopts the hexagonal structure of $P6_3mc$ space group symmetry with lattice constants of $a = b = 5.754$ Å, $c = 5.674$ Å, which consists of triangular Mo clusters and ordered arrays of N atoms [15]. The unit cell is composed of 16 atoms, with eight Mo atoms take the two inequivalent Wyckoff 2*a* (0.000, 0.000, 0.2555) and 6*c* (0.4876, 0.5124, 0.2482) positions, and eight N atoms occupy two inequivalent sites in the Wyckoff 6*c* (0.1667, 0.8333, 0.9934) and 2*b* (0.3333, 0.6667, 0.5203) positions, respectively. The γ-MoN, the cubic phase, crystallizes rather differently from those of hexagonal phases, where both Mo and N atoms occupy sites of square-planar coordination with a simple four-connected three-dimensional (3D) net. It exhibits the NbO-type structure, which can be described as an ordered defected rock-salt structure with one-fourth of the Mo and N atoms missing from the corners and center of the cube. The γ-MoN contains three Mo and three N atoms per unit cell with a lattice constant of $a = b = c = 4.118$ Å. Here the Mo atoms occupy the Wyckoff positions 3*d* (0.500, 0.000, 0.000) and N atoms occupy the 3*c* (0.000, 0.500, 0.500) positions.

*lucheng@calypso.cn

†chen@physics.unlv.edu

Recently, Wang *et al*. [10] synthesized hexagonal δ_3-MoN and cubic γ-MoN through an ion-exchange reaction at moderate pressures up to 5 GPa. They further reported that δ_3-MoN and γ-MoN exhibit excellent hardness of about 30 and 23 GPa at the loads of 0.49 N, and superconducting transition temperature Tc of 13.8 and 5.5 K, respectively. These MoN phases are so far the two hardest known superconducting metal nitrides. The underlying mechanisms for the observed superior hardness remain unexplored at a fundamental level. In the present work, we report a systematic study of the pure and indentation shear strength of all the synthesized MoN phases. The calculated results show that the indentation strength of hexagonal δ_3-MoN is expected to lie between 23.1 and 45.7 GPa, and that for the cubic γ-MoN is 23.0 GPa. These results are in good agreement with the experimentally reported Vickers hardness of about 30 GPa for δ_3-MoN and 23 GPa for γ-MoN [10]. Our findings establish detailed atomistic mechanisms for bond stiffening or softening and bond breaking modes in various MoN phases, which provide a comprehensive description for some anomalous stress responses and unexpected indentation strength variations that stem from the differences in the crystal structures of MoN phases that have the same chemical stoichiometry. These results offer crucial insights for understand fundamental structure-property relations in TM nitrides and may also provide useful guidance for studying other materials, especially the related borides and carbides.

II. COMPUTATIONAL METHODS AND DETAILS

We performed first-principles stress-strain calculations to obtain the ideal pure shear and indentation strength following a computational approach that has been recently developed and applied to many materials [17–25]. The Vienna *ab initio* simulation package (VASP) code [26] was employed, and the total energy calculations and structural relaxations were carried out using the density functional theory (DFT) within the generalized gradient approximation (GGA) [27]. The electron-ion interaction is described by means of projector augmented wave (PAW) method [28] with the $4p^6 4d^5 5s^1$ and $2s^2 2p^3$ electrons treated as valence for Mo and N atoms, respectively. A cutoff energy of 600 eV is used for the plane-wave expansion, together with an adequately fine Monkhorst-Pack k-point sampling [29] in the Brillouin zone. The resulting enthalpy calculations are converged with 1 meV/atom. The quasistatic ideal strength and relaxed loading path in various crystallographic directions are determined using a previously developed method [17–25]. The lattice vectors are incrementally deformed in the direction of the applied strain. At each step the atomic basis vectors and all the atoms inside the unit cell are simultaneously relaxed until all residual components of the Hellmann-Feynman stress tensor orthogonal to the applied strain are less than 0.1 GPa [30]. The shape of the unit cell is determined by the full atomic relaxation without any imposed boundary conditions. To explore the mechanical and dynamic stabilities of the four low-energy phases of MoN, we calculated the elastic constants and phonon dispersion relations under ambient condition. The phonon calculations were performed using a supercell approach as implemented in the PHONOPY code [31]. The obtained elastic constants are listed in Table SI [32]. All structures satisfy the Born-Huang stability criteria [33], indicating their mechanical stability. The calculated elastic constants are somewhat sensitive to the exchange-correlation functionals used in the calculations [32]. The calculated phonon dispersions show that there are no imaginary phonon modes in the entire Brillouin zone in all the cases, thus confirming the dynamic stability of these structures.

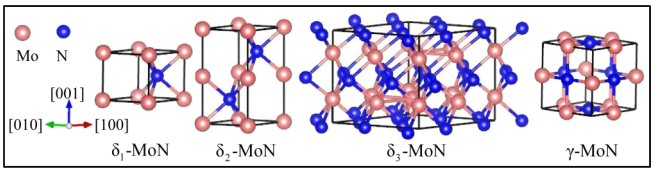

FIG. 1. The crystal structures of the four experimentally synthesized and characterized phases of MoN.

III. RESULTS AND DISCUSSIONS

The Vickers hardness measurements show that the synthesized single crystal δ_3-MoN exhibits a Vickers hardness of ~30 GPa [10]. To assess the experimental results, we calculated stress-strain curves of δ_3-MoN under different loading conditions. Under compressive strains, it is clear that the weakest peak stresses is 76.9 GPa in the $<1\bar{1}0>$ direction. Under tensile strains, the calculated peak stresses are 55.1, 34.3, and 30.5 GPa in the $<001>$, $<110>$, and $<1\bar{1}0>$ directions, respectively, which indicate that $<1\bar{1}0>$ is the weakest tensile direction, and thus the $(1\bar{1}0)$ plane is the easy cleavage plane. Under pure shear strains, $(1\bar{1}0)[001]$ is the lowest shear stress direction, with a peak shear stress of 21.7 GPa, while the other slip directions $(1\bar{1}0)[110]$, $(001)[110]$, $(001)[1\bar{1}0]$, $(110)[001]$, and $(110)[1\bar{1}0]$ have peak stresses of 29.6, 24.8, 22.1, 25.2, and 34.3 GPa, respectively. Thus, the $(1\bar{1}0)$ plane is the easy slip plane for shear deformation of δ_3-MoN.

We now discuss the effect of the normal compressive pressure beneath the (Vickers) indenter on the shear strength of δ_3-MoN in the $(1\bar{1}0)$ crystalline plane, in which both the weakest tensile and pure shear deformations appear. There are two inequivalent shear directions in the $(1\bar{1}0)$ cleavage plane, namely the $(1\bar{1}0)[001]$ and $(1\bar{1}0)[110]$ directions. Calculated results show that the peak stress of δ_3-MoN under Vickers shear are 23.1 GPa (at $\varepsilon = 0.090$) in the $(1\bar{1}0)[001]$ direction and 45.7 GPa (at $\varepsilon = 0.190$) along the $(1\bar{1}0)[110]$ direction. These results suggest that the indentation shear strength of δ_3-MoN is expected to lie between 23.1 and 45.7 GPa, which is in good agreement with the experimentally measured hardness of about 30 GPa [10]. In Fig. 2, we show the calculated stress-strain curves of δ_3-MoN under Vickers shear deformation along the $(1\bar{1}0)[110]$ direction, together with the stress responses under the corresponding pure shear deformations for comparison. Of particular interest are the observation that the ideal indentation strengths are remarkably enhanced compared to the corresponding pure shear strength, with a remarkable strain stiffening effect that brings the ideal strength of δ_3-MoN in the $(1\bar{1}0)[110]$ direction from 29.6 GPa

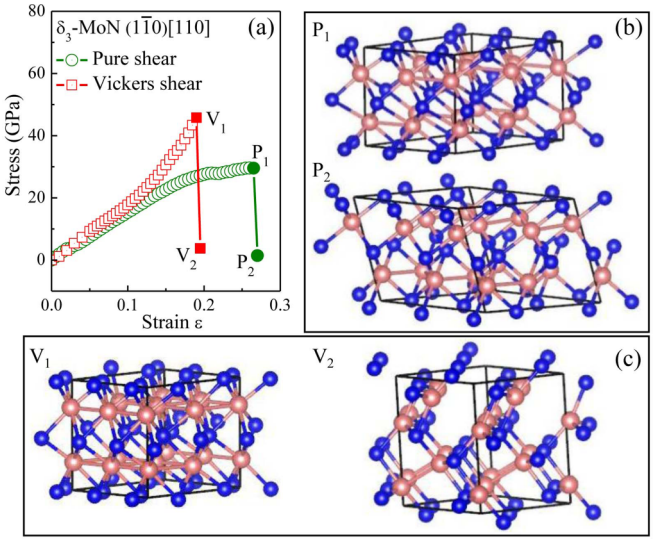

FIG. 2. (a) Calculated stress-strain relations of δ_3-MoN under pure shear and (Vickers) indentation shear along the (1$\bar{1}$0)[110] direction. (b) Selected structural snapshots under the pure shear deformation. (c) Selected structural snapshots under the (Vickers) indentation shear deformation.

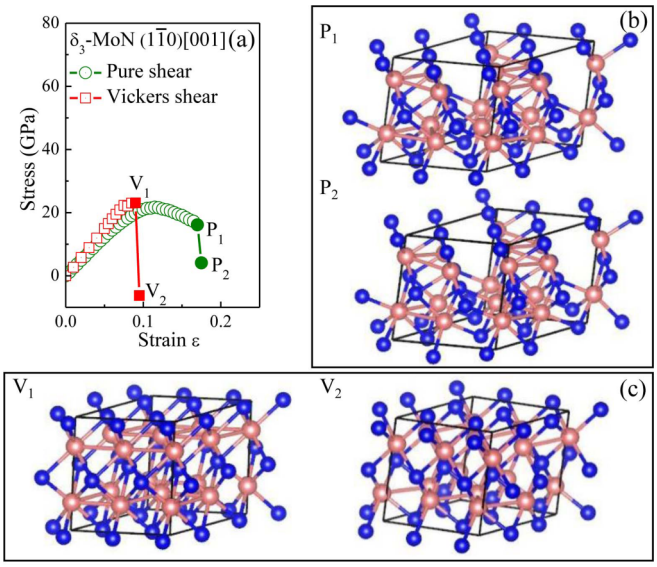

FIG. 3. (a) Calculated stress-strain relations of δ_3-MoN under pure shear and (Vickers) indentation shear along the (1$\bar{1}$0)[001] direction. (b) Selected structural snapshots under the pure shear deformation. (c) Selected structural snapshots under the (Vickers) indentation shear deformation.

at $\varepsilon = 0.260$ under the pure shear to 45.7 GPa at $\varepsilon = 0.190$ under the (Vickers) indentation shear deformation.

To further elucidate the mechanisms underlying the abnormal stress responses and strain stiffening effects that are rarely seen among TM light-element compounds, we plot the structural snapshots of δ_3-MoN under pure shear and (Vickers) indentation shear deformation right before and after the bond breaking strains. At the equilibrium strain $\varepsilon = 0$, the Mo atoms are each coordinated with six N atoms constituting a strongly three-dimensional (3D) trigonal prisms, and part of the Mo atoms, those at the center, form two equilateral triangle with the Mo-Mo bond lengths of 2.663 Å (see Fig. 1), which are shorter than the Mo-Mo bonds in Mo metal (2.800 Å) [34]. Structural snapshots show that, as the pure shear strain increases to 0.260, the Mo-N covalent bonds in the trigonal prisms do not change very much. In contrast, one of the Mo-Mo metallic bonds in the equilateral triangle stretches from 2.663 Å in the intact structure to 2.930 Å, which is larger than 2.800 Å in Mo metal and obviously breaks, and then one of the abscised Mo atoms forms a bent Mo-Mo metallic bond with another adjacent Mo atom, as shown in Fig. 2(b). After passing the peak stress, the Mo-Mo bond flips, and one of the Mo-N covalent bonds in the trigonal prism breaks, leading to the sudden decrease of the shear strength to 1.4 GPa. Under indentation shear deformation, the normal compressive pressure beneath the indenter predominantly compresses the neighboring Mo atoms without appreciably stretching the Mo-N covalent bonds. The Mo-Mo bond lengths decrease from 2.663 Å at $\varepsilon = 0$ to 2.371 Å at $\varepsilon = 0.190$. The rigid linear Mo-Mo metallic bonds, combined with the Mo-N covalent bonds in the trigonal prisms, create a strongly 3D network that is the main load-bearing component and resists large shear deformation under the Vickers indentation loads, which generates a significant enhancement of the indentation strength by more than 54%. As the strain increases to 0.195, the 3D network breaks, as shown in Fig. 2(c), which suddenly releases the indentation stress to 3.7 GPa. Similar phenomena are also seen in δ_3-MoN along the (1$\bar{1}$0)[001] direction under indentation shear deformation. However, the enhancement of the indentation strengths is just 6.5% largely because only part of the linear Mo-Mo bonds are involved in the deformation process, while other bonds are S-shape bent (see Fig. 3).

It is worth noting that the strengths of δ_3-MoN exhibit a large degree of anisotropy along different deformation directions; for example, there is a significant (more than 31.5%) reduction of the shear strength from 34.3 GPa under pure shear to 23.5 GPa under Vickers shear in the (110)[1$\bar{1}$0] direction. The structural changes of δ_3-MoN under pure shear and (Vickers) indentation shear along the (110)[1$\bar{1}$0] direction are displayed in Fig. 4. As the pure shear strain increases to 0.275, corresponding to the maximum shear stress of 34.3 GPa, no Mo-N covalent bonds in the trigonal prisms break. We note, however, that the Mo-Mo metallic bonds in the triangular Mo_3 cluster go through a reconfiguration with the neighboring Mo atoms, resulting in the formation of the linear Mo-Mo metallic bonds along the [010] direction. Meanwhile, as the shear strain further increases to the critical failure strain of 0.285, all the Mo-Mo metallic bonds and one of the Mo-N covalent bonds in the trigonal prisms fracture, releasing the shear stress to 7.3 GPa. In contrast, under indentation shear deformation along the (110)[1$\bar{1}$0] direction, no linear Mo-Mo metallic bonds are formed along the [010] direction, as shown in Fig. 4. Surprisingly, there are linear Mo-Mo metallic bonds in the [110] direction due to the compressive normal stress, but they are not strongly shear resistant together with the Mo-N covalent bonds in the trigonal prisms, and the indentation shear strength only reaches a value of 23.5 GPa and obviously smaller than the pure shear strength of 34.3 GPa. After passing the indentation peak stress, part of the Mo-Mo metallic bonds

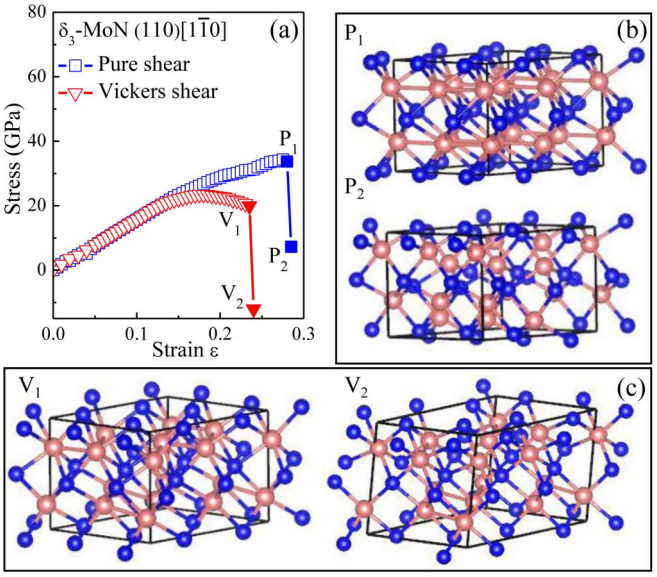

FIG. 4. (a) Calculated stress-strain relations of δ_3-MoN under pure shear and (Vickers) indentation shear along the (110)[1$\bar{1}$0] direction. (b) Selected structural snapshots under the pure shear deformation. (c) Selected structural snapshots under the (Vickers) indentation shear deformation.

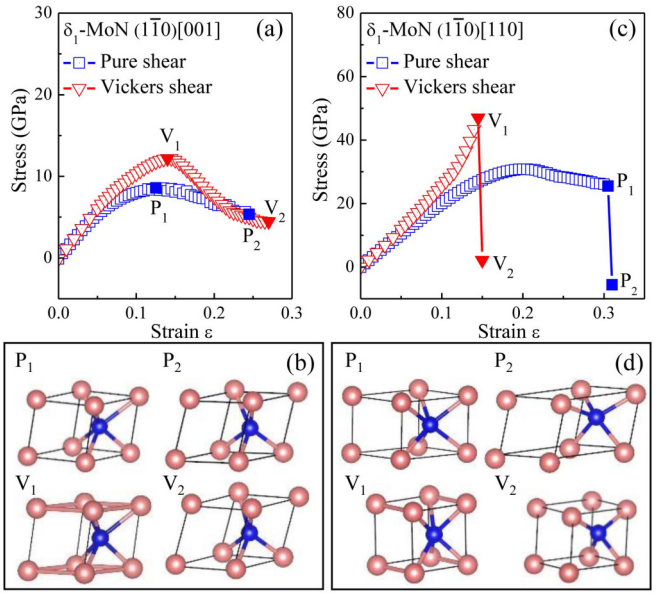

FIG. 5. Calculated stress-strain relations and structural snapshots of δ_1-MoN under pure shear and (Vickers) indentation shear along the two inequivalent directions: (a, b) in the (1$\bar{1}$0)[001] direction, and (c, d) in the (1$\bar{1}$0)[110] direction.

in the [110] direction and the Mo-N covalent bonds in the trigonal prisms are broken with a precipitous drop of stress.

We next examine the deformation mechanism of δ_1-MoN under different loading conditions. Our calculated results show that the minimum peak stress of δ_1-MoN under tensile deformation is 43.1 GPa in the $<1\bar{1}0>$ direction and the weakest peak stress of δ_1-MoN under pure shear strain is 8.6 GPa in the (1$\bar{1}$0)[001] direction. Thus, the (1$\bar{1}$0) plane is the easiest cleavage plane of δ_1-MoN and the (1$\bar{1}$0)[001] direction is the most plausible slip direction of δ_1-MoN. In Fig. 5, we plot the calculated stress-strain curves of δ_1-MoN under pure shear and Vickers shear deformations along the (1$\bar{1}$0)[001] and (1$\bar{1}$0)[110] directions in the (1$\bar{1}$0) cleavage plane. The calculated results clearly show that the ideal strengths of δ_1-MoN in both the (1$\bar{1}$0)[001] and the (1$\bar{1}$0)[110] directions under Vickers shear deformations are higher than those under the corresponding pure shear deformations. The calculated structural snapshots indicate that the load-induced stress enhancement of δ_1-MoN along the two inequivalent shear directions arises from the rigid linear Mo-Mo metallic bond, as shown in Fig. 5. For pure shear deformation, the broking of the Mo-N covalent bonds in the trigonal prisms leads to a shear stress reduction from 8.6 to 5.3 GPa in the (1$\bar{1}$0)[001] direction, and from 25.5 to −5.6 GPa in the (1$\bar{1}$0)[110] direction. Under Vickers shear deformation, δ_1-MoN shows behaviors similar to those seen in δ_3-MoN in the (1$\bar{1}$0) cleavage plane. As the strain increases, the linear Mo-Mo metallic bonds are formed before reaching the failure strain (see Fig. 5) for $\varepsilon = 0.140$ in the (1$\bar{1}$0)[001] and $\varepsilon = 0.145$ in the (1$\bar{1}$0)[110] directions. This leads to a maximum shear stress that is 41.8% larger for the (1$\bar{1}$0)[001] direction and 52.6% higher for the (1$\bar{1}$0)[110] direction than the peak stresses under the corresponding pure shear deformations. After passing the indentation peak stress, part of the Mo-Mo metallic bonds and part of the Mo-N covalent bonds in the trigonal prisms are broken, releasing the accumulated shear stress.

We now turn to the analysis of the stress response for another hexagonal structure of MoN (δ_2-MoN). To determine the deformation mechanism leading to the structure failure of δ_2-MoN, we performed a series of calculations under pure shear deformation by shearing δ_2-MoN along six possible slip directions. Among these six slip directions, the (1$\bar{1}$0)[001] direction has the lowest shear stress of 27.8 GPa at $\varepsilon = 0.135$. Under the (1$\bar{1}$0)[001] indentation shear deformation, the normal pressure beneath the indenter compresses the structure and causes the formation of Mo-Mo metallic bonds, which combine with the Mo-N covalent bonds in the trigonal prisms and eventually lead to greatly enhanced peak shear stress of 34.9 GPa at $\varepsilon = 0.125$ (see Fig. 6). Such indentation induced stiffening also has been found in the (1$\bar{1}$0)[110] direction for δ_2-MoN under indentation shear deformation. The peak stress of δ_2-MoN under the (1$\bar{1}$0)[110] indentation shear strains reaches 59.1 GPa, which is close to the value of cubic BN [35]. This result is attributed to a more dramatic shortening of the Mo-Mo bonds (about 2.300 Å) in the (001) plane when sheared in the [110] direction, which strengthens the bonded framework against the indentation shear deformation. In contrast, the corresponding Mo-Mo bond length is 2.630 Å at the peak-stress strain of $\varepsilon = 0.125$ under the (1$\bar{1}$0)[001] indentation shear deformation.

In addition to these hexagonal structures, Wang *et al*. [10] also reported the synthesis of cubic γ-MoN by slowly heating the sample cell up to 1600° C at 3.5 GPa. The metastable γ-MoN is a major phase coexisting with the hexagonal δ_3-MoN, which also exhibits excellent hardness of about 23 GPa at the load of 0.49 N. We simulated X-ray diffraction (XRD) spectra of all known hexagonal and cubic structures

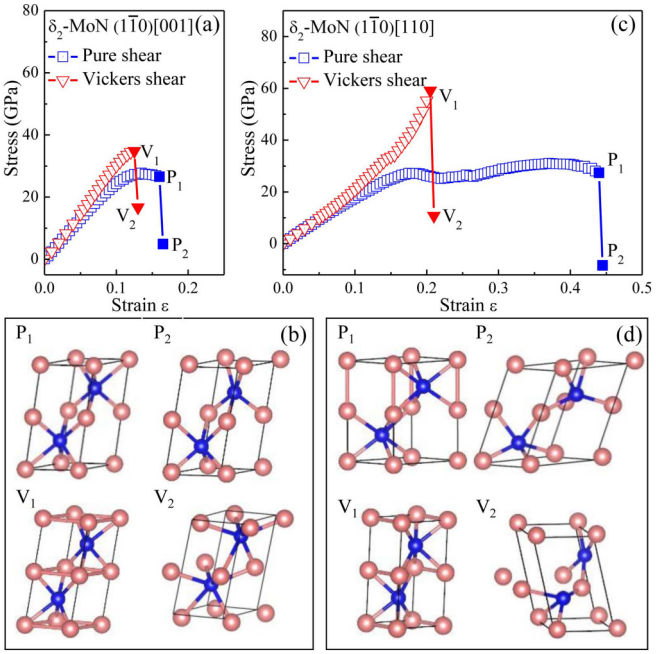

FIG. 6. Calculated stress-strain relations and structural snapshots of δ_2-MoN under pure shear and (Vickers) indentation shear along the two inequivalent directions: (a, b) in the (1$\bar{1}$0)[001] direction, and (c, d) in the (1$\bar{1}$0)[110] direction.

of MoN and compared the results to the experimental XRD pattern. We find an excellent match between simulated and experimental XRD data at ambient condition, as shown in Fig. 7, which indicates that the synthesized cubic γ-MoN possesses the NbO-type structure.

Under tensile strains, the lowest peak stress of γ-MoN is 44.9 GPa along the [001] direction, making the (001) plane the dominant easy cleavage plane. Under pure shear strains, the (001) plane is the most plausible slip plane and the weakest direction is (001)[110] with shear stress of 30.6 GPa. To compare to the indentation hardness results, we examined γ-MoN along several shear directions under indentation shear deformations, and we identified the (001)[110] direction as the weakest shear direction with an (Vickers) indentation strength of 23.0 GPa, which is in excellent agreement with the experimental data [10]. Significantly, despite the same 1:1

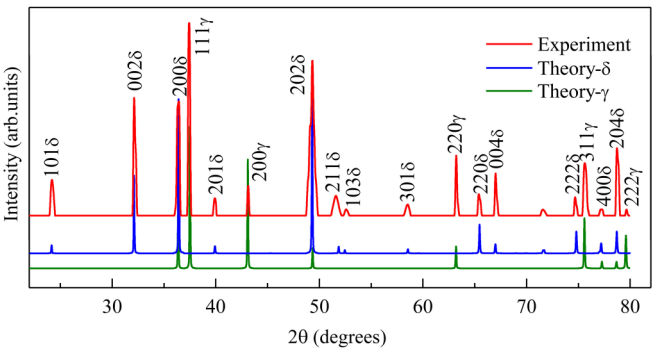

FIG. 7. Simulated and measured [10] XRD patterns of MoN. The experimental XRD patterns are measured at 1300° C.

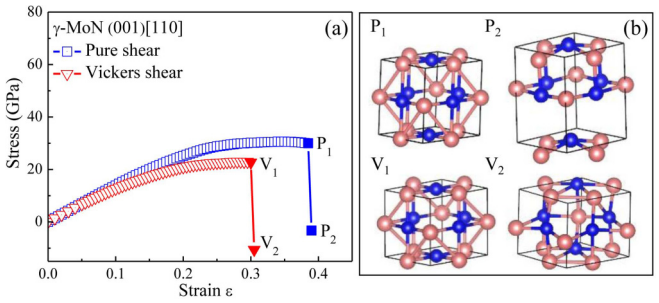

FIG. 8. (a) Calculated stress-strain relations and (b) structural snapshots of γ-MoN under pure shear and (Vickers) indentation shear along the (001)[110] direction.

stoichiometry of Mo and N, the indentation strength of cubic γ-MoN is much lower than those of the hexagonal structures of MoN.

The calculated stress-strain relations and structural snapshots of γ-MoN along the (001)[110] direction under pure shear and indentation shear deformations are shown in Fig. 8. At equilibrium ($\varepsilon = 0$), the center N atoms are each coordinated with four Mo atoms with equivalent Mo-N bond length for 2.059 Å. The deformation process of γ-MoN shearing along the (001)[110] direction shows that, as the pure shear strain increases to 0.385, the Mo-N covalent bonds are stretched from 2.059 to 2.238 Å under shear deformation. In contrast, the distance of the neighboring Mo atoms decreases remarkably from 2.912 Å in the intact structure to 2.653 Å, leading to the formation of new Mo-Mo metallic bonds (see Fig. 8). The four linear Mo-N covalent bonds form a strongly cross-type network and combined with the new Mo-Mo metallic bonds to effectively resist pure shear deformation. Above the strain of 0.385, both Mo-Mo metallic bonds and one of the Mo-N covalent bonds in the cross-type network break, leading to structural failure and reduction of shear stress. The deformation mechanism of γ-MoN under indentation shear deformation in the (001)[110] direction is similar to that under the pure shear deformation, with the formation of the Mo-Mo metallic bonds during the shear process. The indentation strength increases monotonically to a maximum of 23.0 GPa as the shear strain increases to $\varepsilon = 0.280$, and then it reduces slightly to 22.7 GPa at $\varepsilon = 0.300$, where no bonds are broken. The distance between the neighboring Mo atoms decreases to 2.572 Å, and the Mo-Mo metallic bonds form. Finally, we observe that the N atoms gradually sink into the center of the cube leading the linear Mo-N covalent bonds to be bent and a sudden drop of the indentation shear stress at $\varepsilon = 0.305$.

To examine how the structural and chemical bonding changes affect the indentation strength, we compared the stress-strain relations and the associated bond breaking mechanism of the four crystal structures of MoN. The above calculated results reveal that the [1$\bar{1}$0] direction is the weakest tensile direction for δ_1-MoN and δ_3-MoN, while the weakest tensile direction for the δ_2-MoN is the [110] direction, and for the cubic structure γ-MoN it is the [001] direction. The lowest pure shear stress peaks of the three hexagonal structures of MoN are all along the (1$\bar{1}$0)[001] direction with the values of 8.6 GPa for δ_1-MoN, 27.8 GPa for δ_2-MoN, and

21.7 GPa for δ_3-MoN. However, the lowest pure shear stress peaks of the cubic structure γ-MoN is 30.6 GPa along the (001)[110] direction, which is obviously higher than those of the hexagonal structures. This is because that both the Mo and N atoms in cubic γ-MoN occupy sites of the square-planar coordination and the four linear Mo-N covalent bonds form a strongly cross-type network that combined with the Mo-Mo metallic bonds can effectively resist pure shear deformation. In contrast, the Mo-N covalent network in the hexagonal structures of MoN are distinctly weaker under the pure shear deformations.

Our study shows that all the MoN phases in hexagonal structures, i.e., δ_1-MoN, δ_2-MoN, and δ_3-MoN, exhibit significant strain stiffening that produces considerably enhanced indentation strengths, especially in the $(1\bar{1}0)[110]$ direction where the indentation strength exceeds 40 GPa, which is the threshold value commonly set for superhard materials. This remarkable hardness enhancement is attributed to the presence of the rigid linear Mo-Mo metallic bonds, which combine with the Mo-N covalent bonds in the trigonal prisms in the hexagonal structure to create a strongly 3D network that effectively resists large shear deformation under Vickers indentation strains. In contrast, the cubic γ-MoN shows a strain softening under all the indentation shear deformations with a reduction in shear strength at large strains. In particular, the ideal indentation strengths of MoN in the $(1\bar{1}0)[001]$ direction is reduced by more than 56%. This contrasting behavior is attributed to that the cubic γ-MoN has large vacancies at the corners and in the center of the cubic cell, which reduces the ability of γ-MoN to resist large shear deformation under Vickers indentation strains. Meanwhile, we also find strain softening phenomena in the hexagonal structures of MoN under various shear directions. Such strength reductions stem from the anisotropic nature of the linear Mo-Mo metallic bonds that are unable to resist large strains along certain weak directions despite their ability to do much better in the strong directions. Furthermore, it is also interesting to note that the ideal indentation strengths of δ_2-MoN and δ_3-MoN are visibly larger than that of δ_1-MoN. Specifically, the strengths are 34.9 GPa at $\varepsilon = 0.125$ for δ_2-MoN $>$ 23.1 GPa at $\varepsilon = 0.090$ for δ_3-MoN $>$ 12.2 GPa at $\varepsilon = 0.140$ for δ_1-MoN, which is consistent with the structural data showing the same trend in the lengths of the Mo-Mo metallic bonds: 2.630 Å (δ_2-MoN) $>$ 2.672 Å (δ_3-MoN) $>$ 2.806 Å (δ_1-MoN).

To further confirm the reliability of the above-mentioned results, we test the stress-strain curves of hexagonal δ_3-MoN along the $(1\bar{1}0)[001]$ direction and cubic γ-MoN along the (001)[110] direction under pure shear and indentation shear deformations by using different exchange-correlation functionals, such as generalized gradient approximation with Hubbard U parameter (GGA + U), local density approximation (LDA), and local density approximation with Hubbard U parameter (LDA + U). Overall, the peak values of hexagonal δ_3-MoN along the $(1\bar{1}0)[001]$ direction and cubic γ-MoN along the (001)[110] direction under pure shear and indentation shear deformations are almost unchanged by considering the coulomb interaction of the Mo 4d electrons. The calculated peak values by LDA functional are, about 5.0 GPa, higher than those of GGA and GGA + U functionals, however, the trend of stress-strain curves are the same. The detailed results are shown in the Supplemental Material [32].

IV. CONCLUSION

We performed systematic first-principles calculations to examine the stress responses, especially under pure and indentation shear strains that are most relevant to the experimental hardness measurements, for four reportedly synthesized crystal phases of MoN along various deformation modes. The calculated results show that crystal structural symmetry and the associated bonding configurations play an important role in determining key mechanical properties of crystalline solids, including those with the same chemical stoichiometry as in the present case. As a result, the three hexagonal structures of MoN share some common trends and similar stress-strain relations. These include the strong anisotropy in their peak stresses along various crystallographic directions and abnormal strain-stiffening effect in the $(1\bar{1}0)$ cleavage plane under Vickers indentation deformations. The strain stiffening behavior is attributed to the rigid linear Mo-Mo metallic bonds between the adjacent MoN_6 octahedra, which is combined with the Mo-N covalent bonds to create a strongly 3D bonding network that is capable of resisting large shear deformations under Vickers indentation strains. In contrast, the cubic structure of γ-MoN shows nearly isotropic stress response and a drastically contrasting strain softening phenomenon along all crystallographic directions. In this later case, the normal pressure beneath the indenter drives the face-centered N atoms to sink into the vacancies of the γ-MoN crystal lattice, which further weakens the Mo-N bonds. This effect leads to a considerably reduced strength of cubic γ-MoN, producing an ideal indentation strength of 23 GPa, which is in good agreement with the measured Vickers hardness, while the measured value of 30 GPa for hexagonal δ_3-MoN is considerably (30%) higher. These insights expand the fundamental understanding of atomistic mechanisms underlying the experimentally measured hardness, which is directly related to the indentation strength [17–25], and the associated structural deformation of various MoN phases. The present findings also provide useful guidelines for further exploring novel TM nitrides, borides, and carbides, especially distinguishing and identifying among many distinct crystal structures with rich bonding configurations those that are most likely to possess superior mechanical properties under diverse loading conditions.

ACKNOWLEDGMENTS

This work was supported, in part, by National Natural Science Foundation of China under Grants No. U1804121 and No. 11304167.

[1] M. Bykov, S. Chariton, H. Z. Fei, T. Fedotenko, G. Aprilis, A. V. Ponomareva, F. Tasnádi, I. A. Abrikosov, B. Merle, P. Feldner, S. Vogel, W. Schnick, V. B. Prakapenka, E. Greenberg, M. Hanfland, A. Pakhomova, H. P. Liermann, T. Katsura, N. Dubrovinskaia, and L. Dubrovinsky, High-pressure synthesis of ultraincompressible hard rhenium nitride pernitride $Re_2(N_2)(N)_2$ stable at ambient conditions, Nat. Commun. **10**, 2994 (2019).

[2] J. Deng, N. Liu, J. G. Guo, and X. L. Chen, Large spin gaps in the half-metals MN_4 (M=Mn, Fe, Co) with N_2 dimers, Phys. Rev. B **99**, 184409 (2019).

[3] K. R. Babu and G. Y. Guo, Electron-phonon coupling, superconductivity, and nontrivial band topology in NbN polytypes, Phys. Rev. B **99**, 104508 (2019).

[4] S. Wang, H. Ge, S. Sun, J. Zhang, F. Liu, X. Wen, X. Yu, L. Wang, Y. Zhang, H. Xu, J. C. Neuefeind, Z. Qin, C. Chen, C. Jin, Y. Li, D. He, and Y. Zhao, A new molybdenum nitride catalyst with rhombohedral MoS_2 structure for hydrogenation applications, J. Am. Chem. Soc. **137**, 4815 (2015).

[5] B. Biswas and B. Saha, Development of semiconducting ScN, Phys. Rev. Mater. **3**, 020301 (2019).

[6] X. Zheng, H. Wang, X. Yu, J. Feng, X. Shen, S. Zhang, R. Yang, X. Zhou, Y. Xu, R. Yu, H. Xiang, Z. Hu, C. Jin, R. Zhang, S. Wei, J. Han, Y. Zhao, H. Li, and S. Wang, Magnetic origin of phase stability in cubic γ-MoN, Appl. Phys. Lett. **113**, 221901 (2018).

[7] K. Niwa, T. Yamamoto, T. Sasaki, and M. Hasegawa, High-pressure synthesis, crystal growth, and compression behavior of hexagonal CrN_2 having one-dimensionally aligned nitrogen dime, Phys. Rev. Mater. **3**, 053601 (2019).

[8] A. F. Young, C. Sanloup, E. Gregoryanz, S. Scandolo, R. J. Hemley, and H. K. Mao, Synthesis of Novel Transition Metal Nitrides IrN_2 and OsN_2, Phys. Rev. Lett. **96**, 155501 (2006).

[9] B. Alling, T. Marten, and I. A. Abrikosov, Questionable collapse of the bulk modulus in CrN, Nat. Mater. **9**, 283 (2010).

[10] S. Wang, D. Antonio, X. Yu, J. Zhang, A. L. Cornelius, D. He, and Y. Zhao, The hardest superconducting metal nitride, Sci. Rep. **5**, 13733 (2015).

[11] L. B. Craig, F. M. Paul, S. Emmanuel, and L. Kurt, Determination of the crystal structure of δ-MoN by neutron diffraction, J. Solid State Chem. **177**, 1488 (2004).

[12] A. Gomathi, A. Sundaresan, and C. N. R. Rao, Nanoparticles of superconducting γ-Mo_2N and δ-MoN, J. Solid State Chem. **180**, 291 (2007).

[13] X. Zhao and K. J. Range, High pressure synthesis of molybdenum nitride MoN, J. Alloys Compd. **296**, 72 (2000).

[14] F. Fujimoto, Y. Nakane, M. Satou, F. Komori, K. Ogata, and Y. Andoh, Formation of molybdenum nitride films by ion beam and vapor deposition method, Nucl. Instrum. Methods Phys. Res., Sect. B **19**, 791 (1987).

[15] M. B. Kanoun, S. Goumri-Said, and M. Jaouen, Structure and mechanical stability of molybdenum nitrides: A first-principles study, Phys. Rev. B **76**, 134109 (2007).

[16] K. Balasubramanian, L. P. Huang, and D. Gall, Phase stability and mechanical properties of $Mo_{1-x}N_x$ with $0 \ll x \ll 1$, J. Appl. Phys. **122**, 195101 (2017).

[17] C. Lu, Q. Li, Y. Ma, and C. Chen, Extraordinary Indentation Strain Stiffening Produces Superhard Tungsten Nitrides, Phys. Rev. Lett. **119**, 115503 (2017).

[18] B. Li, H. Sun, and C. Chen, Extreme Mechanics of Probing the Ultimate Strength of Nanotwinned Diamond, Phys. Rev. Lett. **117**, 116103 (2016).

[19] Q. Li, D. Zhou, W. Zheng, Y. Ma, and C. Chen, Anomalous Stress Response of Ultrahard WB_n Compounds, Phys. Rev. Lett. **115**, 185502 (2015).

[20] M. Zhang, H. Liu, Q. Li, B. Gao, Y. Wang, H. Li, C. Chen, and Y. Ma, Superhard BC_3 in Cubic Diamond Structure, Phys. Rev. Lett. **114**, 015502 (2015).

[21] B. Li, H. Sun, and C. Chen, Large indentation strain stiffening in nanotwinned cubic boron nitride, Nat. Commun. **5**, 4965 (2014).

[22] B. Li, H. Sun, C. Zang, and C. Chen, Fundamental constraints on the strength of transition-metal borides: The case of CrB_4, Phys. Rev. B **87**, 174106 (2013).

[23] C. Zang, H. Sun, and C. Chen, Unexpectedly low indentation strength of WB_3 and MoB_3 from first principles, Phys. Rev. B **86**, 180101 (2012).

[24] C. Zang, H. Sun, J. S. Tse, and C. Chen, Indentation strength of ultraincompressible rhenium boride, carbide, and nitride from first-principles calculations, Phys. Rev. B **86**, 014108 (2012).

[25] W. Zhou, H. Sun, and C. Chen, Soft Bond-Deformation Paths in Superhard γ-Boron, Phys. Rev. Lett. **105**, 215503 (2010).

[26] G. Kresse and J. Furthmüller, Efficient iterative schemes for *ab initio* total-energy calculations using a plane-wave basis set, Phys. Rev. B **54**, 11169 (1996).

[27] J. P. Perdew, J. A. Chevary, S. H. Vosko, K. A. Jackson, M. R. Pederson, D. J. Singh, and C. Fiolhais, Atoms, molecules, solids, and surfaces: Applications of the generalized gradient approximation for exchange and correlation, Phys. Rev. B **46**, 6671 (1992).

[28] P. E. Blöchl, Projector augmented-wave method, Phys. Rev. B **50**, 17953 (1994).

[29] H. J. Monkhorst and J. D. Pack, Special points for Brillonin-zone integrations, Phys. Rev. B **13**, 5188 (1976).

[30] Z. Pan, H. Sun, Y. Zhang, and C. Chen, Harder than Diamond: Superior Indentation Strength of Wurtzite BN and Lonsdaleite, Phys. Rev. Lett. **102**, 055503 (2009).

[31] A. Togo, F. Oba, and I. Tanaka, First-principles calculations of the ferroelastic transition between rutile-type and $CaCl_2$-type SiO_2 at high pressures, Phys. Rev. B **78**, 134106 (2008).

[32] See Supplemental Material at http://link.aps.org/supplemental/10.1103/PhysRevMaterials.4.044002 for the technical details of the stress-strain relations, calculated elastic constants, and selected stress-strain curves of MoN.

[33] Z. Wu, E. Zhao, H. Xiang, X. Hao, X. Liu, and J. Meng, Crystal structures and elastic properties of superhard IrN_2 and IrN_3 from first principles, Phys. Rev. B **76**, 054115 (2007).

[34] R. Marchand, F. Tessier, and F. J. DiSalvo, New routes to transition metal nitrides: preparation and characterization of new phases, J. Mater. Chem. **9**, 297 (1999).

[35] Y. Zhang, H. Sun, and C. Chen, Structural deformation, strength, and instability of cubic BN compared to diamond: A first-principles study, Phys. Rev. B **73**, 144115 (2006).